Journal of Mechanics in Medicine and Biology

Accepted August 27th 2016

Print ISSN: 0219-5194
Online ISSN: 1793-6810
IMPACT FACTOR = 0.797

PUBLISHER: WORLD SCIENTIFIC (SINGAPORE)

ANALYTICAL STUDY OF ELECTRO-OSMOSIS MODULATED CAPILLARY PERISTALTIC HEMODYNAMICS

[1]Dharmendra Tripathi, [1]Shashi Bhushan and ***[2]O. Anwar Bég**

[1]Department of Mechanical Engineering, Manipal University, Jaipur-303007, India.
[2] Fluid Dynamics, Bio-Propulsion and Nanosystems, Department of Mechanical and Aeronautical Engineering, Salford University, Newton Building, The Crescent, Salford, M54WT, England, UK.

ABSTRACT

A mathematical model is developed to analyse electro-kinetic effects on unsteady peristaltic transport of blood in cylindrical vessels of finite length. The Newtonian viscous model is adopted. The analysis is restricted under Debye-Hückel linearization (i.e. wall zeta potential ≤ 25mV) is sufficiently small). The transformed, non-dimensional conservation equations are derived via lubrication theory and long wavelength and the resulting linearized boundary value problem is solved exactly. The case of a thin electric double layer (i.e. where only slip electro-osmotic velocity considered) is retrieved as a particular case of the present model. The response in pumping characteristics (axial velocity, pressure gradient or difference, volumetric flow rate, local wall shear stress) to the influence of electro-osmotic effect (inverse Debye length) and Helmholtz-Smoluchowski velocity is elaborated in detail. Visualization of trapping phenomenon is also included and the bolus dynamics evolution with electro-kinetic effects examined. A comparative study of train wave propagation and single wave propagation is presented under the effects of thickness of EDL and external electric field. The study is relevant to electrophoresis in haemotology, electrohydrodynamic therapy and biomimetic electro-osmotic pumps.

Keywords: *Electro-osmosis; axial electric field; finite length tube; Debye Length; microfluidics; trapping; capillary hemodynamics, viscous flow; biomimetic blood pumps.*

**Corresponding author* - *email: O.A.Beg@salford.ac.uk; gortoab@gmail.com*

1. INTRODUCTION

In recent years great interest has developed in transporting erythrocytes and proteins through micro-capillaries electro-kinetically using longitudinal (axially-directed) electric fields [**1**]. Electro-kinetics also has immense possible applications in the synthesis of novel chip-based miniaturized medical diagnostic kits [**2**], separation dynamics in blood disorder treatment and endothelial electrophysiology [**3**], electrogenic bioplasma transport [**4**], continuous-flow electro-kinetic-assisted plasmapheresis [**5**], electro-osmotic manipulation of DNA in microfabricated systems [**6**] and dielectrophoretic manufacture of biopolymers [**7**]. Electro-kinetics provides a rich arena for multi-physical simulations. It combines viscous flow, electro-physics and depending on the geometry via which the transport takes place, a variety of rich boundary conditions (moving wall, oscillatory, micro-channel, transpiration, adhesion etc). Ghosal [**8**] has provided a lucid review of applications in capillary transport, emphasizing that careful selection of different chemical, electrical and viscous conditions can benefit dispersion rates. In conjunction with the many excellent laboratory-based investigations which have been reported on capillary electro-kinetics and electro-hemodynamics [**9**], theoretical and computational studies have also stimulated exceptional interest in recent years. Simulation has therefore evolved into a very key area of modern electro-osmotic fluid dynamics research. The presence of ionic components, nutrients and other particles in blood, which respond to bio-electrical and also externally applied electrical fields, provides a suitable forum for electro-kinetic simulations in hemodynamics. In many narrow vessel or microchannel applications, electrokinetic flow fields can be delineated into an internal flow domain controlled by viscous and electrostatic forces and an external flow domain regulated by inertial and pressure forces. These two regions are demarcated via a slip velocity condition which is determined by the Helmholtz−Smoulochowski equation. Many aspects of dielectric phenomena, polarizability, mobility of ions and Debye length effects have been addressed comprehensively by Sharp and Honig [10] who have also covered in detail finite difference numerical simulations of a standard model in electro-kinetics, the Poisson-Boltzmann equation. Liu *et al.* [11] developed a robust 3D immersed molecular electrokinetic finite element method (**IMEFEM**) to simulate micro fluidic electrokinetic assemblies of bio-molecules, blood transport and related problems including pH control interactions. They described bio-sensing efficiency, applied electric field threshold, biomolecule deformation and nanoscale Brownian motion. Hlushkou *et al.* [12] presented a modified lattice-Boltzmann method for three-dimensional electroosmotic flows in porous

media, specifically addressing electro-kinetics in straight cylindrical capillaries with a non-uniform zeta-potential distribution for ratios of the capillary inner radius to the thickness of the electrical double layer from 10 to 100. Sheu *et al.* [13] investigated computationally and experimentally electro-osmotic blood flows in ionic tissue model, as a simulation of the meridian passage, elaborating on immediate response and electrical field interaction with the blood circulation. Gheshlaghi *et al.* [14] developed closed-form Fourier series solutions to transient electro-kinetic flow in a parallel rotating plate microchannel, noting that period and the decay rate of the oscillations are invariant with the Debye-Hückel parameter and that a complex time dependent boundary layer structure at the channel walls evolves at greater rotational frequencies. Furthermore they observed that both angular velocity and the Debye-Hückel parameters strongly modify the induced transient secondary (cross) flow. Santiago [15] investigated theoretically the influence of effects of fluid inertia and pressure on the velocity and vorticity field of electroosmotic insulated wall channel flows, considering Strouhal number effects. Alam and Penney [16] described a Lagrangian methodology for simulating electro-osmotic mass diffusion in microchannels studying behaviour at high Peclet numbers. Luo *et al.* [17] employed a combination of smoothed profile method (SPM) and spectral element discretizations, to study electro-kinetic flows in both straight channels and charged micro-tubular cylinders, considering variations in electrical conductivities between the charged surfaces and electrolyte solution. Bég *et al.* [18] studied non-linear electro-kinetic flows in circular tubes using a Chebyschev spectral method, considering electrical Reynolds number, electrical Hartmann and electrical slip effects. They observed that electrical Hartmann number decelerates the ionic flow whereas increasing electrical Reynolds number enhances the electrical field distribution. Huang *et al.* [19] investigated electroosmotic dynamics in micro-channels with a modified finite element method. They solved the coupled mass, momentum, Laplace (equation for the effective electrical potential) and Helmholtz (electrical potential in the electric double layer i.e. EDL) equations at Re=0.0259), observing that greater applied electric potential accelerates the tissue fluid owing to the formation of an EDL. Karatay *et al.* [20] analysed using the CFD-ACE commercial solver and a direct numerical simulation (DNS) code, the electro-convective flow induced by concentration polarization near an ion selective surface, computing in detail the velocity and ion concentration spectra over many frequencies. They also observed that DNS codes compile faster than commercial codes solvers in electro-osmotic coupled simulations. Ondal *et al.* [21] investigated the combined electroosmotic and pressure driven flow in a rectangular microchannel at high zeta potential and with an overlapping electrical double-layer. They

conducted computational simulations to compute the potential distribution without the conventional Debye Huckel approximation with a site dissociation model.

The above studies were generally confined to *steady state* flows with rigid boundaries. However most transport processes in physiology are *transient* e.g. pusaltile effects due to the beating of the heart. An important unsteady propagation mechanisms for transport is *peristalsis* which is a radially symmetrical contraction and relaxation of muscles that propagates materials in a wave-like motion along a conduit utilizing deformable walls. This mechanism arises in an astonishing range of biological systems including pharyngeal physiology [**22**], vasomotion (periodic oscillations of blood vessels walls) in bat wing venules [**23**], pulmonary and perivascular space (PVS) dynamics [**24**], bile migration in the gastric tract [**25**]. Peristalsis has also been implemented in several bio-inspired medical devices including nano-scale pharmacological delivery systems [**26, 27**], fish locomotion for underwater robots [**28**] and biomimetic worm soft peristaltic land crawling robots [**29, 30**]. Although documented for over a century in medical sciences, fundamental studies of *peristaltic hydrodynamics* only materialized in the 1960s. The premier researcher in biomechanics, Y.C. Fung with co-workers presented a seminal investigation on the subject [**31**]. This study considered peristaltic pumping generated via the imposition of an axisymmetric traveling sinusoidal wave of moderate amplitude on the wall of a flexible conduit. The nonlinear convective acceleration terms in the Navier-Stokes equation were retained and perturbation solutions developed. Further studies of Newtonian peristaltic propulsion considering different aspects including inertial, elastic wall and activation waves were communicated by Weinberg *et al.* [**32**], Tang and Rankin [**33**], Carew and Pedley [**34**] and Tang and Shen [**35**].

The above studies although very detailed, were restricted to *infinite length geometries*. However the vast majority of real applications of peristalsis involve *finite length* channels, vessels etc. An important work considering transient peristaltic flows in finite length conduits was presented by Li and Brasseur [**36**]. Kumar *et al*. [**37**] extended the Li-Brasseur model to consider wall permeability. Tripathi and Bég [**38**] further consider hydromagnetic peristaltic flow and thermal convection heat transfer in a finite length channel observing that higher pressure is needed to drive electrically-conducting Newtonian fluids compared with non-conducting Newtonian fluids, whereas, a lower pressure is necessary when strong thermal buoyancy effects are present. Toklu [**39**] presented a detailed simulation of esophageal bolus transport in a finite intraluminal geometry integrating actual videofluoroscopic and

concurrent manometric geometric data with a viscous Newtonian numerical model. Further studies of finite length conduit peristalsis have been communicated by Tong *et al*. [**40**], Pal and Brasseur [**41**] in the context of uro-dynamics and by Jaggy *et al.* [**42**] for the peristaltic, extracorporeal displacement pump (Affinity) employed in cardiopulmonary bypass hemodynamics.

In the present article we consider *electro-osmotic Newtonian viscous peristaltic pumping in a finite length geometry*. Although numerous studies have been communicated on *magnetohydrodynamic* peristalsis e.g. [**44**], relatively few investigations have appeared on *electro-kinetic or electro-osmotic peristaltic transport*. Bandopadhyay *et al*. [**45**], motivated by microscale device synthesis, recently considered peristaltic electro-osmotic flows of aqueous electrolytes under applied electric fields, evaluating the influence of electro-kinetic body force on the particle reflux and trapping of a fluid volume (bolus) inside the travelling wave. Misra *et al.* [**45**] investigated analytically the electroosmotic flow of a micropolar fluid in a microchannel with permeable walls under periodic vibration. Tripathi *et al.* [**46**] reported on the combined magnetiohydrodynamic and electro-osmotic unsteady peristaltic propulsion of electrolytes in a microchannel under an applied external electric field observing that with higher magnetic Hartmann number, the formation of bolus in the regime (associated with trapping) is opposed up to a critical value of magnetic field. They also found that stronger electro-osmotic effect (i.e. lower Debye length) enhances maximum time-averaged flow rate but induces axial deceleration. Goswami *et al*. [**47**] studied the pumping characteristics of electro-kinetically modulated peristaltic transport of power-law fluids tin narrow deformable channels showing that principal influence of electro-osmosis is in weakly peristaltic flow and that trapping can be regulated via electric field. Further relevant studies include Johnson [**48**] who micro-machined a four-chamber peristaltic electro-osmotic pump and McKnight *et al.* [**49**] who considered electrode effects on peristaltic electro-kinetic pumping. In the present work analytical solutions are derived for the axial velocity, pressure and stream-function using integral methods. Numerical visualization of trapping phenomena under electro-osmotic effect is achieved with Mathematica software. The present study aims to further examine peristaltic electro-osmotic hemodynamics with finite length geometric effects. Lubrication theory is applied and a long wave approximation is used [peristaltic wavelength is much greater amplitude, which eliminates nonlinear convective acceleration terms from the Navier-Stokes equations) and with Debye-Huckel linearization, permits the derivation of closed-form solutions to the transformed boundary value problem. The work is motivated by applications in

ionic diffusion and blood pumping with peristaltic waves in cerebro-spinal zones [**50**] and potential biomimetic devices exploiting such mechanisms [**51, 52**]. It may also relevant to electrofluid botanical transport [**53**]. The mathematical model of Li and Brasseur [**36**] is retrieved as a very special case of the present general model.

2. ELECTRO-OSMOTIC PERISTALTIC VISCOUS HEMODYNAMIC MODEL

We consider the blood flow through capillary as microfluidic circular cylindrical tube where blood is an aqueous ionic solution and may be manipulated by means of an externally applied electric field. Electro-hydrodynamic properties of blood have been well established in many landmark physiological studies. Blood flow is known to generate a concomitant electrical force that acts within the blood vessel–the electrokinetic vascular streaming potential (EVSP). This amazing phenomenon was first identified by the prominent German physiologist, Quincke [**54**] in the 1860s. More recently with developments in electro-osmotic systems, the electro-hemodynamic phenomenon has been exploited in many other areas including vascular control [**55**], hemostasis [**56**], wound repair [**57**] and cerebral electro-therapy [**58**]. Ionic concentrations within blood and surface charges in haemotological vessels are primarily responsible for electro-kinetic effects which generate electrical body forces that can be manipulated via external electrical fields. We also consider the tube (blood vessel) to be of finite length, and the propulsion processes to be inherently *non-steady* in the laboratory frame of reference. The schematic of the problem under consideration is depicted in **Fig. 1** and mathematically described by the following expression

$$\bar{h}(\bar{x},\bar{t}) = a - \bar{\phi}\cos^2\frac{\pi}{\lambda}(\bar{x}-c\bar{t}) \quad \forall\, x \in [0,\, L], \tag{1}$$

where $a, \bar{\phi}, \lambda, \bar{x}, c, \bar{t}, L$ are the radius of tube, amplitude, wavelength, axial coordinate, wave velocity, time and tube length. The *Poisson-Boltzmann* equation to describe the electric potential distribution for a symmetric (*z*: *z*) binary electrolyte solution (Na^+ Cl^-), is expressed as:

$$\nabla^2\bar{\Phi} = -\frac{\bar{\rho}_e}{\varepsilon}, \tag{2}$$

Here ε is the permittivity and ρ_e is the density of the total ionic change which is given by, $\rho_e = ez(n^+ - n^-)$, in which n^+ and n^- are the number of densities of cations and anions, respectively.

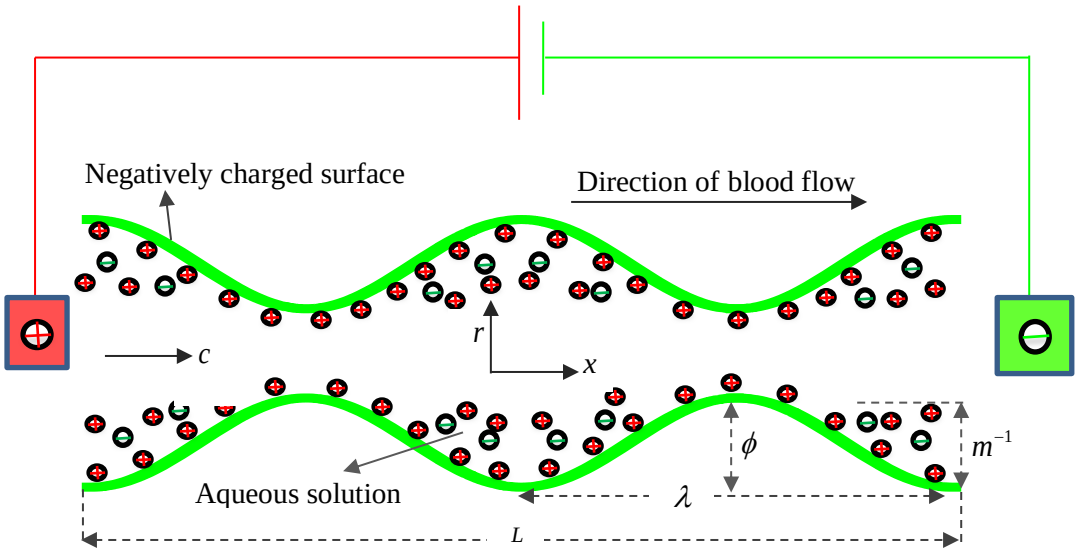

Figure 1: A geometrical description of peristaltic blood flow through the capillary augmented by external electric field. The pressures at the left and right reservoirs (inlet and exit, respectively) are denoted as p_0 and p_L respectively.

The density of the total ionic energy (considering no EDL overlap) is expressed as:

$$n^{\pm} = n_0 Exp\left[\pm \frac{e\, z\, \bar{\Phi}}{K_B T}\right], \tag{3}$$

where n_0 represents the concentration of ions at the bulk, which is independent of surface electro-chemistry, e is the electronic charge, z is charge balance, K_B is the Boltzmann constant, T is the average temperature of the electrolytic solution. This distribution of ionic concentration appears to be valid when there is *no axial gradient of the ionic concentration* within the micro-channel and the flow Péclet number is assumed to be significantly small. Combining Eqns. (2) and (3), we obtain the *modified Poisson-Boltzmann equation* in the form:

$$\frac{1}{\bar{r}} \frac{\partial}{\partial \bar{r}} \left(\bar{r} \frac{\partial \bar{\Phi}}{\partial \bar{r}} \right) = \frac{2 n_0 ez \sinh\left(\frac{ez\bar{\Phi}}{K_B T} \right)}{\varepsilon}. \tag{4}$$

Invoking a normalized electro-osmotic potential function $\bar{\Phi}$ with zeta potential ζ of the medium along with other non-dimensional variables, namely $\Phi = \frac{\bar{\Phi}}{\zeta}$ and $r = \frac{\bar{r}}{a}$ (radial coordinate) and employing the Debye-Hückel linearization approximation as $\sinh\left(\frac{ez\Phi}{K_B T}\right) \approx \frac{ez\Phi}{K_B T}$, Eqn. (4) may be shown to contract to:

$$\frac{1}{r}\frac{\partial}{\partial r}\left(r\frac{\partial \Phi}{\partial r}\right) = m^2\Phi, \tag{5}$$

where $m = aez\sqrt{\frac{2n_0}{\varepsilon K_B T}} = \frac{a}{\lambda_d}$, is the electro-osmotic i.e. electro-kinetic parameter which is the inverse of the Debye length, λ_d. It is important to note that when the zeta (ζ) potential is significant or the background electrolyte is weak, the electric double layer (EDL) can grow strongly in thickness and over-lapping may arise. Furthermore if the EDL takes up a substantial portion of the channel, velocity profiles can be modified local and the electrostatic body force could lead to the expulsion of counter-ions (to the surface charge). These extreme aspects have been elaborated by Saville [**59**]. However in the present analysis we do not consider thick EDLs. These are deferred to a subsequent study will be no longer be plug shaped, and the Solving Eq.(5) subjected to the boundary conditions: $\left.\frac{\partial \Phi}{\partial r}\right|_{r=0} = 0$ and $\Phi|_{r=h} = 1$, the potential function is obtained as:

$$\Phi = \frac{I_0(mr)}{I_0(mh)}, \tag{6}$$

where $I_0(mr)$ is the modified Bessel function of first kind and zero order [**60**].

The governing equations describing time-dependent, viscous Newtonian electro-osmotic blood flow through a deformable capillary under an applied external electric field may be presented in an axisymmetric coordinate system ($\bar{r}, \bar{x}$) as:

$$\frac{\partial \bar{u}}{\partial \bar{x}} + \frac{1}{\bar{r}}\frac{\partial(\bar{r}\bar{v})}{\partial \bar{r}} = 0, \tag{7}$$

$$\rho\left(\frac{\partial}{\partial \bar{t}}+\bar{u}\frac{\partial}{\partial \bar{x}}+\bar{v}\frac{\partial}{\partial \bar{r}}\right)\bar{u}=-\frac{\partial \bar{p}}{\partial \bar{x}}+\mu\left(\frac{\partial^2 \bar{u}}{\partial \bar{x}^2}+\frac{1}{\bar{r}}\frac{\partial}{\partial \bar{r}}\left(\bar{r}\frac{\partial \bar{u}}{\partial \bar{r}}\right)\right)+\bar{\rho}_e E_x, \quad (8)$$

$$\rho\left(\frac{\partial}{\partial \bar{t}}+\bar{u}\frac{\partial}{\partial \bar{x}}+\bar{v}\frac{\partial}{\partial \bar{r}}\right)\bar{v}=-\frac{\partial \bar{p}}{\partial \bar{r}}+\mu\left(\frac{\partial^2 \bar{v}}{\partial \bar{x}^2}+\frac{\partial}{\partial \bar{r}}\left(\frac{1}{\bar{r}}\frac{\partial(\bar{r}\bar{v})}{\partial \bar{r}}\right)\right), \quad (9)$$

where $\rho, \bar{u}, \bar{v}, \bar{p}, \mu,$ and E_x denote the fluid density, axial velocity, radial velocity, pressure, fluid viscosity, and external electric field, respectively. Although it is possible to derive numerical solutions for the primitive equations (subject to boundary conditions), it is advantageous to invoke non-dimensional parameters. These allow a proper scaling of electro-kinetic flow phenomena and greatly simplify the complexity of the governing equations. Proceeding, we define:

$$x=\frac{\bar{x}}{\lambda}, t=\frac{c\bar{t}}{\lambda}, u=\frac{\bar{u}}{c}, v=\frac{\bar{v}}{c\delta}, \delta=\frac{a}{\lambda}, h=\frac{\bar{h}}{a}, \phi=\frac{\bar{\phi}}{a}, p=\frac{\bar{p}a^2}{\mu c\lambda}, \mathrm{Re}=\frac{\rho c a}{\mu}, \quad (10)$$

where $\delta,$ is wave number, and *Re* is the *wave amplitude and capillary-diameter based-*Reynolds number. Eqns. (7) –(9) then take the form:

$$\frac{\partial u}{\partial x}+\frac{1}{r}\frac{\partial(rv)}{\partial r}=0, \quad (11)$$

$$\mathrm{Re}\,\delta\left(\frac{\partial}{\partial t}+u\frac{\partial}{\partial x}+v\frac{\partial}{\partial r}\right)u=-\frac{\partial p}{\partial x}+\left(\delta^2\frac{\partial^2 u}{\partial x^2}+\frac{1}{r}\frac{\partial}{\partial r}\left(r\frac{\partial u}{\partial r}\right)\right)+m^2\Phi U_{HS}, \quad (12)$$

$$\mathrm{Re}\,\delta^3\left(\frac{\partial}{\partial t}+u\frac{\partial}{\partial x}+v\frac{\partial}{\partial r}\right)v=-\frac{\partial p}{\partial r}+\delta^2\left(\delta^2\frac{\partial^2 v}{\partial x^2}+\frac{\partial}{\partial r}\left(\frac{1}{r}\frac{\partial(rv)}{\partial r}\right)\right), \quad (13)$$

where $U_{HS}=-\frac{E_x\varepsilon\zeta}{\mu c}$ is the Helmholtz-Smoluchowski velocity. It is assumed that the wavelength of the pulse is much larger than the radius of tube; i.e. we assume that the lubrication approximation is valid *(δ = a/λ<<1*). Applying these approximations the governing equations finally assume a much more compact and amenable form:

$$\frac{\partial u}{\partial x}+\frac{1}{r}\frac{\partial(rv)}{\partial r}=0, \quad (14)$$

$$\frac{\partial p}{\partial x}=\frac{1}{r}\frac{\partial}{\partial r}\left(r\frac{\partial u}{\partial r}\right)+m^2U_{HS}\frac{I_0(mr)}{I_0(mh)}, \quad (15)$$

$$\frac{\partial p}{\partial r} = 0. \tag{16}$$

Eqns. (15) and (16) evidently correspond to a non-zero axial pressure gradient and zero radial pressure gradient, respectively. The relevant boundary conditions, following Li and Brasseur [**36**] are prescribed as follows:

$$\left.\frac{\partial u}{\partial r}\right|_{r=0} = 0\,,\ u\big|_{r=h} = 0,\ v\big|_{r=0} = 0\ v\big|_{r=h} = \frac{\partial h}{\partial t}\,,\ p\big|_{x=0} = p_0\,,\ \ p\big|_{x=L} = p_L\,. \tag{17}$$

Solving Eqn.(15) with boundary conditions (17), the *electro-kinetic modified axial velocity* is obtained as:

$$u = \frac{1}{4}\frac{\partial p}{\partial x}\left(r^2 - h^2\right) - U_{HS}\left\{\frac{I_0(mr)}{I_0(mh)} - 1\right\}. \tag{18}$$

Using the Eqn. (18) and boundary condition (17), the *electro-kinetically modulated radial velocity* by virtue of the continuity equation is found to be:

$$v = \frac{r}{4}\left\{-\frac{\partial^2 p}{\partial x^2}\left(\frac{r^2}{4} - \frac{h^2}{2}\right) + h\frac{\partial p}{\partial x}\frac{\partial h}{\partial x}\right\} - U_{HS}\,\frac{I_1(mr)\,I_1(mh)}{(I_0(mh))^2}\frac{\partial h}{\partial x}, \tag{19}$$

where $I_1(mr)$ is the modified Bessel function of first kind of first order (see Kreyzig [**60**]).

Using Eq.(19) and boundary conditions (17), the *pressure gradient* is obtained as:

$$\frac{\partial p}{\partial x} = \frac{1}{h^4}\left[G_0(t) + 16\int_0^x\left\{h\frac{\partial h}{\partial t} + U_{HS}\,h\frac{\partial h}{\partial s}\left(\frac{I_1(mh)}{I_0(mh)}\right)^2\right\}ds\right], \tag{20}$$

where $G_0(t)$ is arbitrary function of t to be evaluated by using *finite length* boundary conditions (17). The *pressure difference* can be computed along the axial length by:

$$p(x,t) - p(0,t) = \int_0^x \frac{\partial p}{\partial s}ds\,, \tag{21}$$

and $G_0(t)$ is expressed as:

$$G_0(t) = \frac{(p_l - p_0) - 16\int_0^L h^{-4}\int_0^x\left\{h\frac{\partial h}{\partial t} + U_{HS}\,h\frac{\partial h}{\partial s}\left(\frac{I_1(mh)}{I_0(mh)}\right)^2\right\}dsdx}{\int_0^L h^{-4}dx}. \tag{22}$$

The local wall shear stress is defined again following Li and Brasseur [**36**]:

$$\tau_w = \left.\frac{\partial u}{\partial r}\right|_{r=h} = \frac{1}{2}\frac{\partial p}{\partial x}h - U_{HS}\frac{mI_1(mh)}{I_0(mh)}. \tag{23}$$

The *volumetric flow rate* is defined as:

$$Q(x,t) = 2\int_0^h urdr = -\frac{h^4}{8}\frac{\partial p}{\partial x} + U_{HS}\left(h^2 - \frac{2hI_1(mh)}{mI_0(mh)}\right). \tag{24}$$

The pumping performance is characterized for periodic train waves by averaging the volumetric flow rate for one time interval i.e. *time-averaged volume flow rate*. This is defined following Shapiro *et al.* [**61**] as:

$$\bar{Q} = \int_0^1 Qdt = Q - h^2 + 1 - \phi + 3\phi^2/8. \tag{25}$$

Using Eqns. (24) and (25), the *pressure gradient* is derived in the form of time-averaged flow rate as:

$$\frac{\partial p}{\partial x} = \frac{8}{h^4}\left\{(1 - \bar{Q} - h^2 - \phi + 3\phi^2/8) + U_{HS}\left(h^2 - \frac{2hI_1(mh)}{mI_0(mh)}\right)\right\}. \tag{26}$$

Using Eqns. (18) and (19), the *stream function in the wave frame* (obeying the Cauchy-Riemann equations, $u = \frac{1}{r}\frac{\partial \psi}{\partial r}$ and $v = -\frac{1}{r}\frac{\partial \psi}{\partial x}$) takes the form:

$$\psi = \frac{1}{16}\frac{\partial p}{\partial x}(r^4 - 2r^2h^2) - U_{HS}\left(\frac{rI_1(mr)}{mI_0(mh)} - \frac{r^2}{2}\right). \tag{27}$$

All the above expressions will reduce to the Newtonian viscous expressions in the absence of electro-osmosis, of Li & Brasseur [**36**] for $U_{HS} = 0$ i.e. without external electrical field. The derived solutions will also reduce to expressions for thin EDL effects (i.e. only electroosmotic slip velocity at the wall is considered, neglecting external electric field effects) which is a special case of this study for $m \to \infty$ or where thickness of the EDL tends to zero ($\lambda_d \to 0$).

3. NUMERICAL RESULTS AND DISCUSSION

Figs.2-10 depict the influence of the electro-osmotic parameter ($m = aez\sqrt{\frac{2n_0}{\varepsilon K_B T}} = \frac{a}{\lambda_d}$), (which is inversely proportional to Debye length (λ_d) or characteristic thickness of electrical double layer (EDL)) *and* Helmholtz-Smoluchowski (HS) velocity ($U_{HS} = -\frac{E_x \varepsilon \zeta}{\mu c}$), (which is proportional to external electric field (E_x)),on the pumping characteristics of blood flow and associated trapping dynamics. The other parameters $\varepsilon, \zeta, \mu, c$ (i.e. permittivity, zeta potential, dynamic viscosity and peristaltic wave velocity) are held constant. All numerical solutions were evaluated and graphical plots generated using Mathematica software

Figs. 2(a-d) illustrate the effect of inverse Debye length i.e. electro-osmotic parameter, on pressure distribution at four time instants (t = 0, 0.25 ,0.5, 0.75) for both train and single wave propagations along the length of tube. The initial and final pressure ($p_0 = p_L = 0$) are taken as zero in the numerical calculation and dual waves are propagating together for train wave propagation case. The length of tube is twice the wavelength. The figures indicate that the maximum blood pressure arises for fully contracted walls whereas the minimum is associated with fully relaxed walls. It is clear that due to contraction and relaxation of walls, there exists a *negative pressure gradient* and this causes the forward propagation of the blood bolus (trapped vorticity zone). For figs. 2(a-d), we have taken the status of bolus at different instants which visualizes the rhythmic process of fluid transportation. It is also observed that the pressure increases with increasing the thickness of Debye length in train wave propagation while opposite trends are observed for single wave propagation.

Figs. 3(a-d) present the effects of external electric field (as simulated via variation in the Helmholtz-Smoluchowski (HS) velocity, U_{HS}), on pressure distribution for train and single wave propagation along the tube length at different time instants. Pressure is clearly greater in blood flow without external electric field. Pressure is *strongly reduced* therefore via increasing the magnitude of external electrical field for *train wave propagation*. However the influence of external field on pressure for single wave propagation is opposite to that of the train wave propagation and pressures are found to be elevated. The patterns of pressure distribution without external electric field are consistent with the pattern of pressure distribution given by Li and Brasseur [**36**] providing confidence in the current analytical solutions. Numerical values in the Li-Brasseur results are different however since both the

equation for peristaltic wave propagation and parameter values are different. However the general trends are quite similar for non-electrical peristalsis.

Figs. 4(a-d) show the evolution in local wall shear stress distribution along the tube length for train wave propagation and single wave propagation at different time instants under the effects of electro-osmotic parameter (m) i.e. inverse Debye length (λ_d). There is a significant depression at all time stages in the shear stress with increasing m values. The blood flow is therefore strongly decelerated with greater electro-osmotic effect, which concurs with many other studies in this area, notably Goswami *et al*. [**47**]. The alternating nature of wall shear stress induced by the peristaltic wave is clearly captured in these figures.

Figs. 5a-d illustrate the impact of Helmholtz-Smoluchowski velocity on the local wall shear stress along the length of tube at $\phi = 0.5, L = 2, p_L = p_0 = 0, m = 2$ at different time instants (a) $t = 0,1$ (b) $t = 0.25$ (c) $t = 0.5$ (d) $t = 0.75$. Solid and dashed colour lines represent the local wall shear stress for different values. Initial and final pressure ($p_0 = p_L = 0$) are taken as zero in the numerical calculations and two waves are propagating together for the train wave propagation case and a single wave is propagating along the tube length.

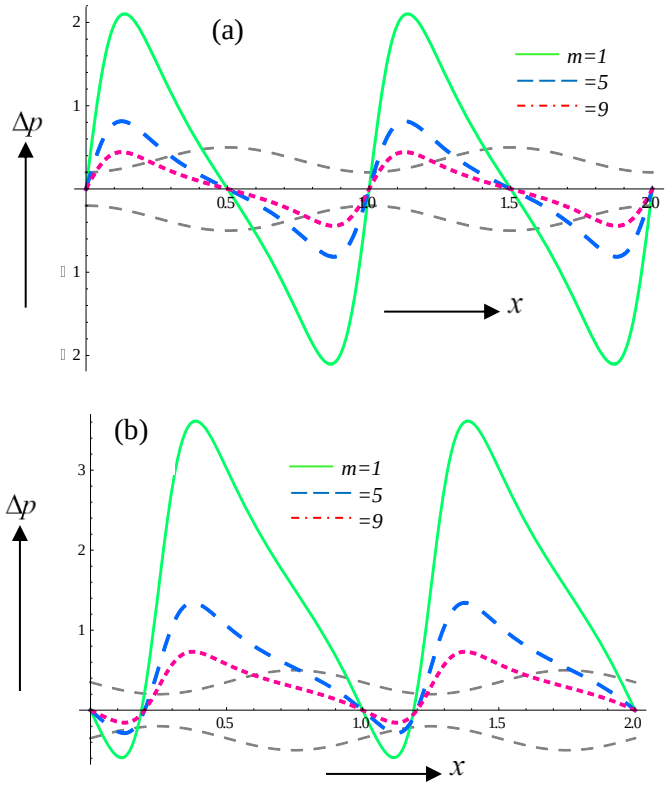

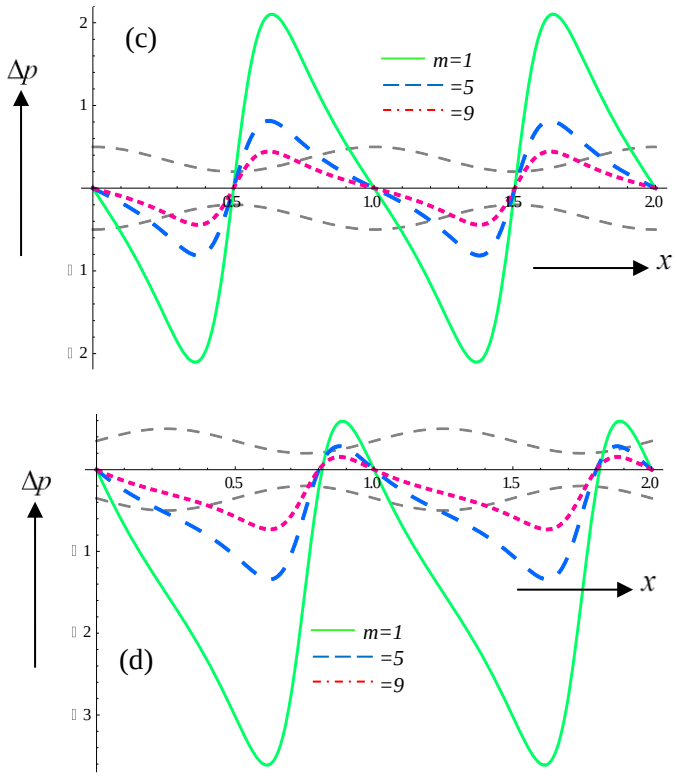

Fig.2. Pressure distribution along the length of tube at $\phi = 0.6, L = 2, p_L = p_0 = 0, U_{HS} = 1$ at different time instants (a) $t = 0,1$ (b) $t = 0.25$ (c) $t = 0.5$ (d) $t = 0.75$. Solid and dashed colour lines represent the pressure distribution for different values of electroosmotic parameter (inverse Debye length) and dotted black lines show the pulse position.

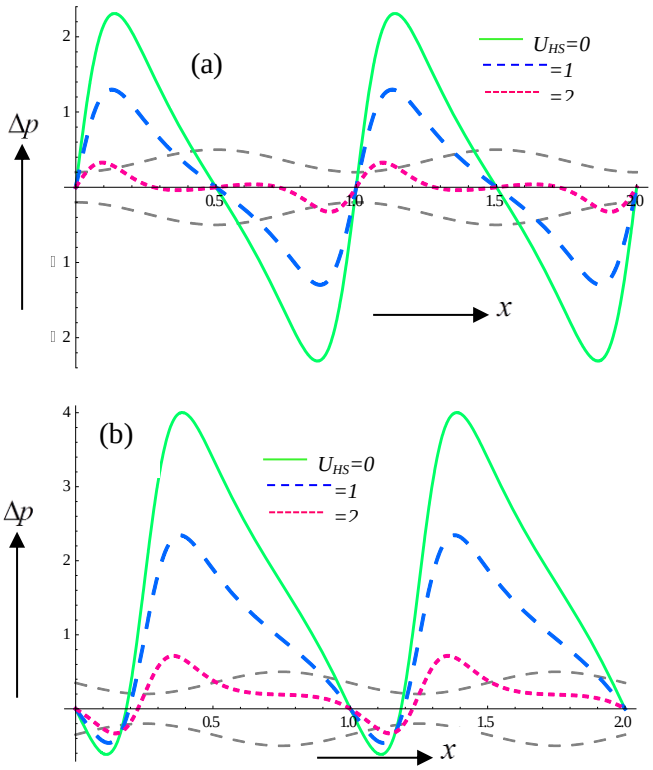

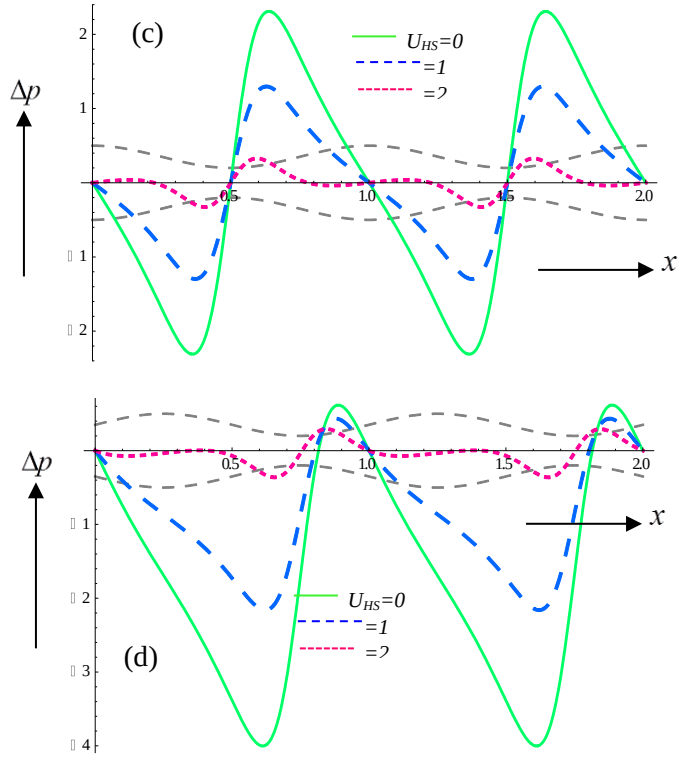

Fig.3. Pressure distribution along the length of channel at $\phi = 0.6, L = 2, p_L = p_0 = 0, m = 3$ at different time instants (a) $t = 0{,}1$ (b) $t = 0.25$ (c) $t = 0.5$ (d) $t = 0.75$. Solid and dashed colour lines represent the pressure distribution for different values of Helmholtz-Smoluchowski velocity and dotted black lines show the pulse position.

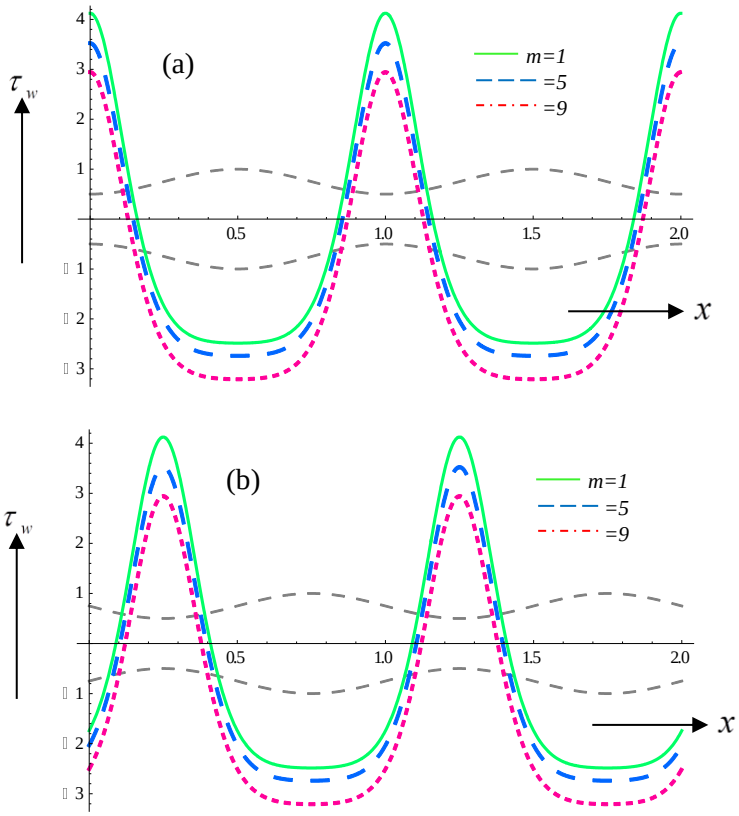

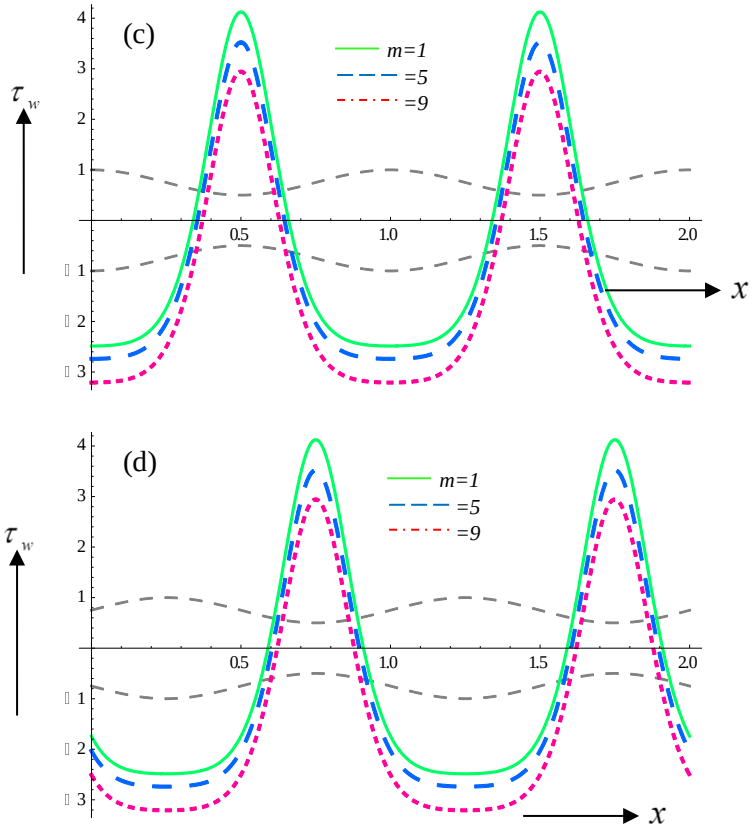

Fig.4. Local wall shear stress along the length of tube at $\phi = 0.5, L = 2, p_L = p_0 = 0, U_{HS} = 0.1$ at different time instants (a) $t = 0{,}1$ (b) $t = 0.25$ (c) $t = 0.5$ (d) $t = 0.75$. Solid and dashed colour lines represent the local wall shear stress for different electro-osmotic parameter (inverse Debye lengths) and dotted black lines show pulse position.

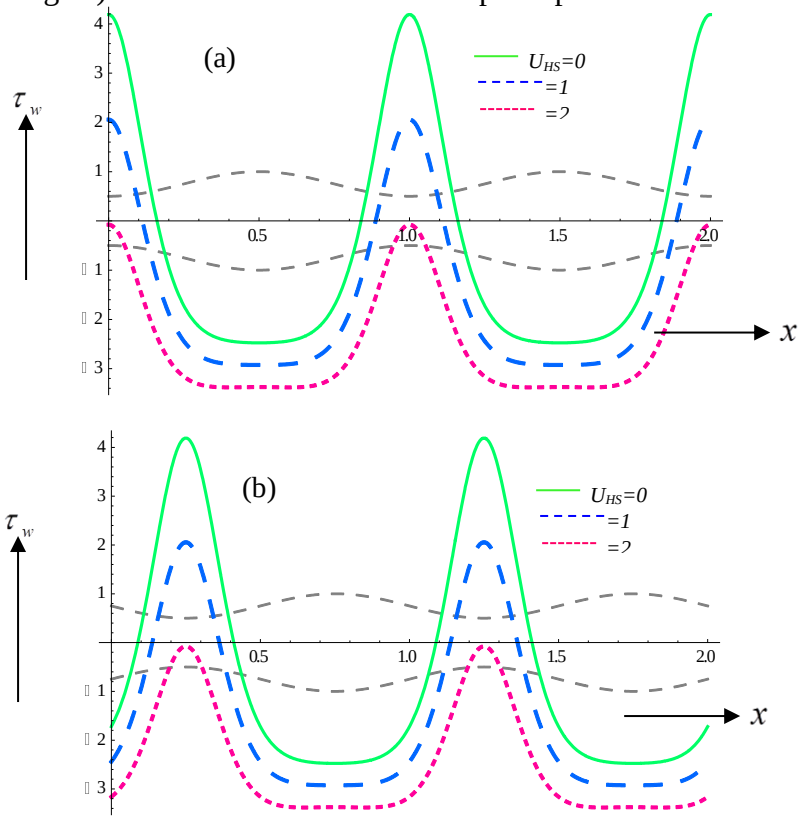

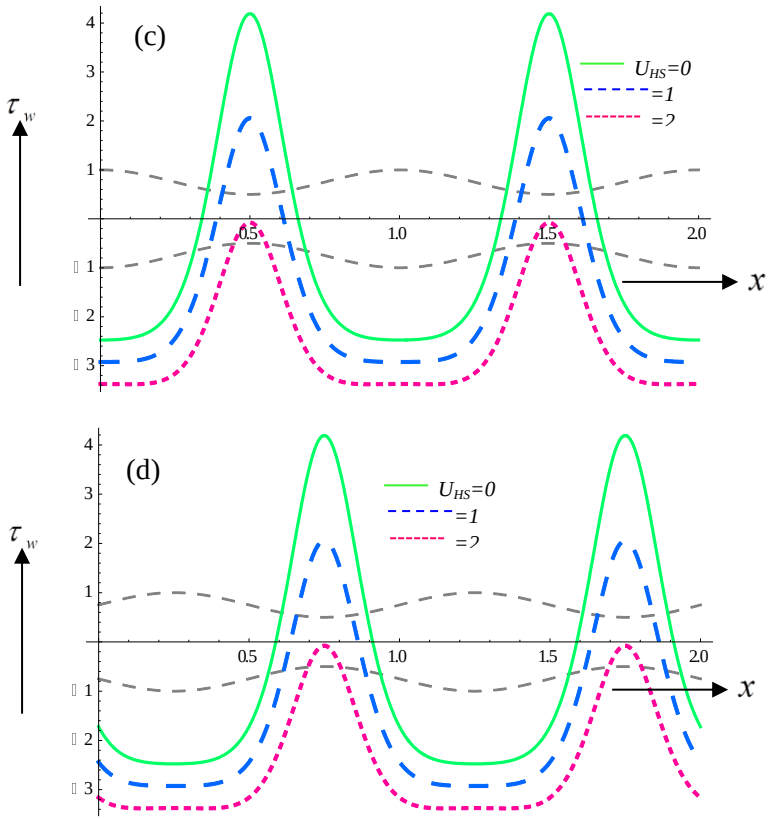

Fig.5. Local wall shear stress along the length of tube at $\phi = 0.5, L = 2, p_L = p_0 = 0, m = 2$ at different time instants (a) $t = 0{,}1$ (b) $t = 0.25$ (c) $t = 0.5$ (d) $t = 0.75$. Solid and dashed colour lines represent the local wall shear stress for different values of Helmholtz-Smoluchowski velocity and dotted black lines show pulse position.

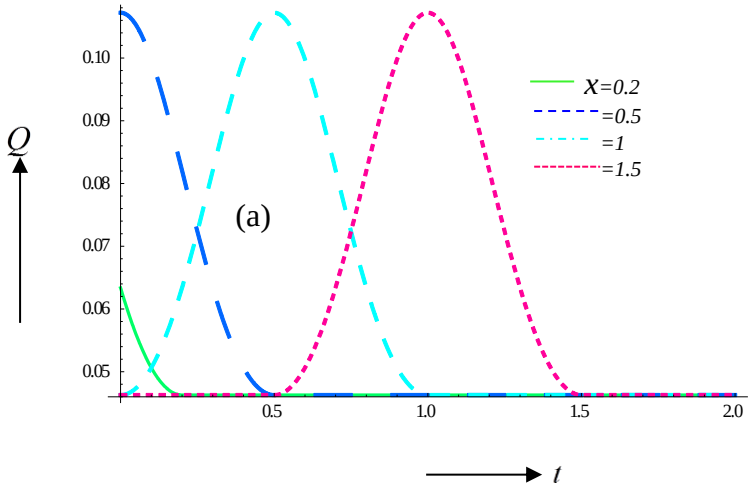

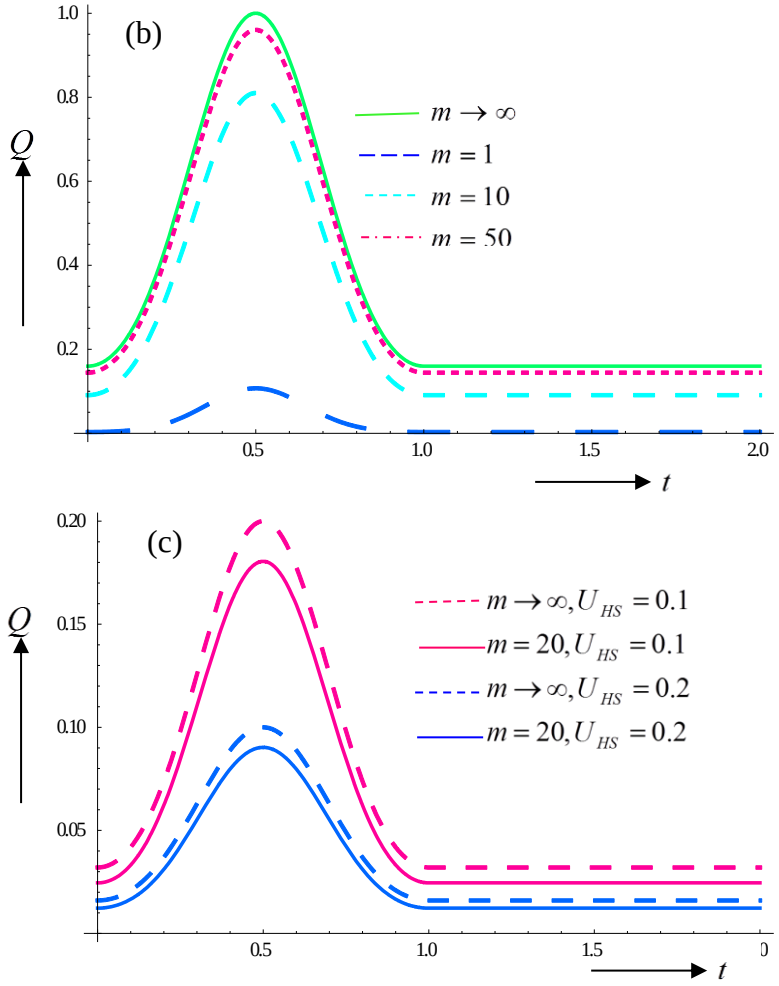

Fig.6. Volumetric flow rate against the time for pulse flow at $\phi = 0.6, p_x = 0,$ (a) for axial distance (x), with $m = 1, U_{HS} = 1$ from inlet to outlet (b) for different values of electro-osmotic parameter (inverse Debye length) (c) for different values of electro-osmotic parameter (inverse Debye length) and Helmholtz-Smoluchowski velocity.

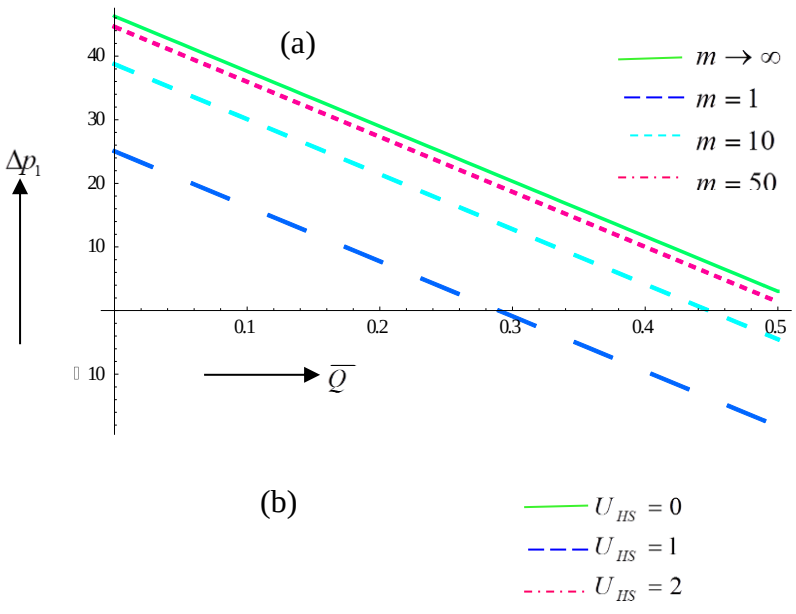

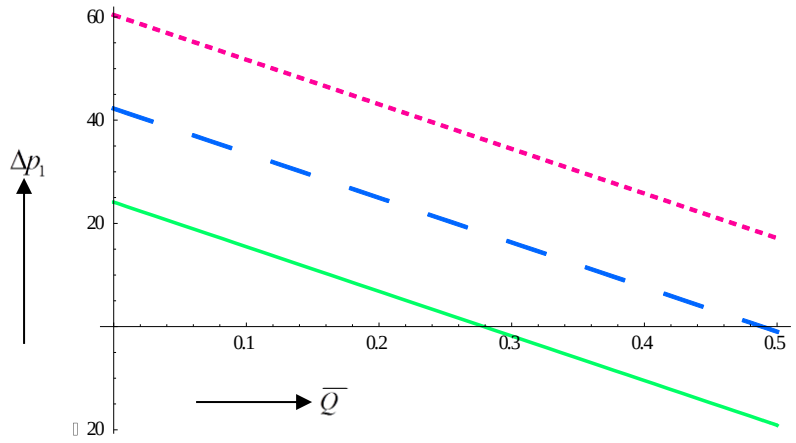

Fig.7. Pressure difference across one wavelength vs. time averaged flow rate at $\phi = 0.6$ and (a) $U_{HS} = 1$ (b) $m = 20$.

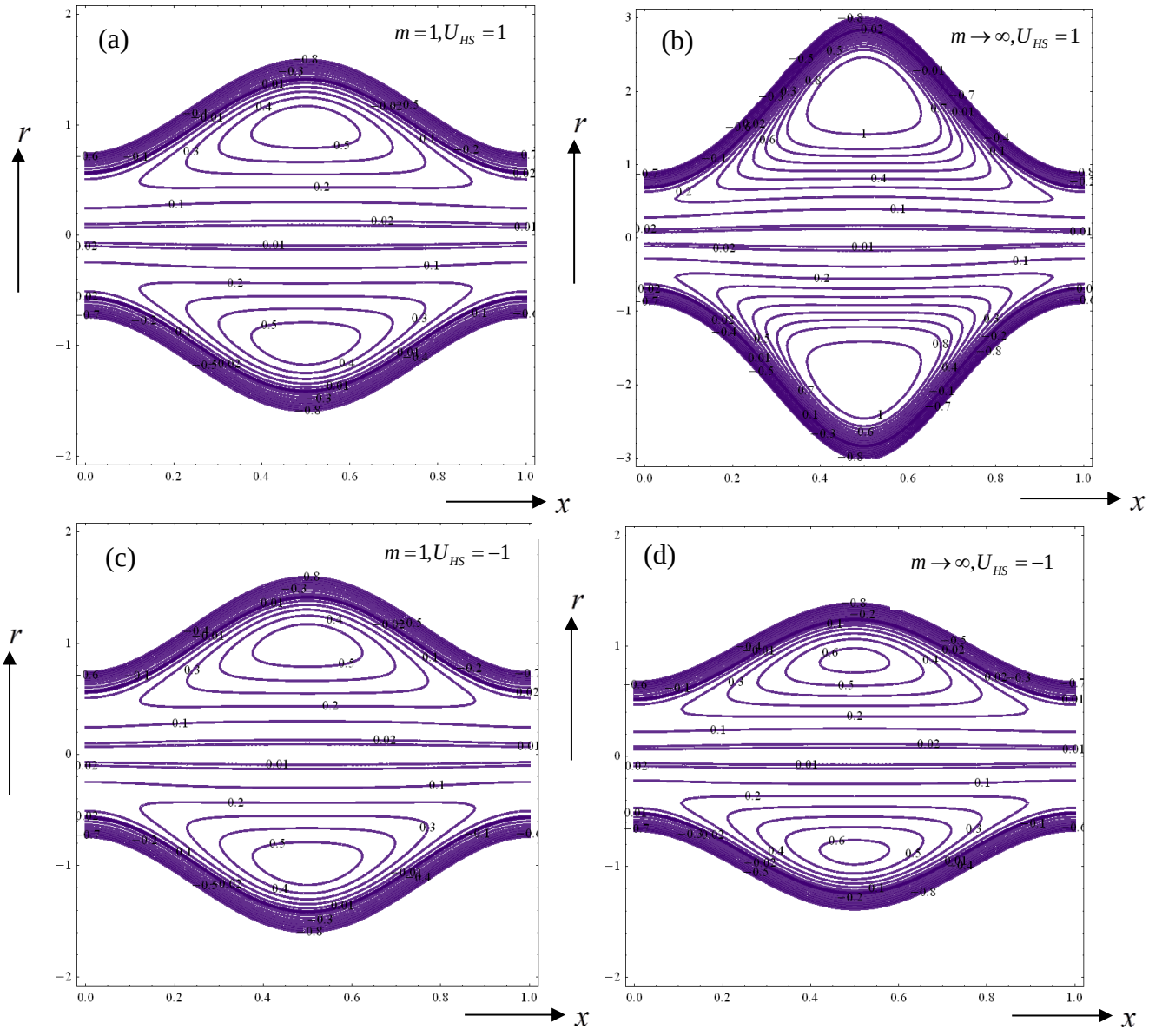

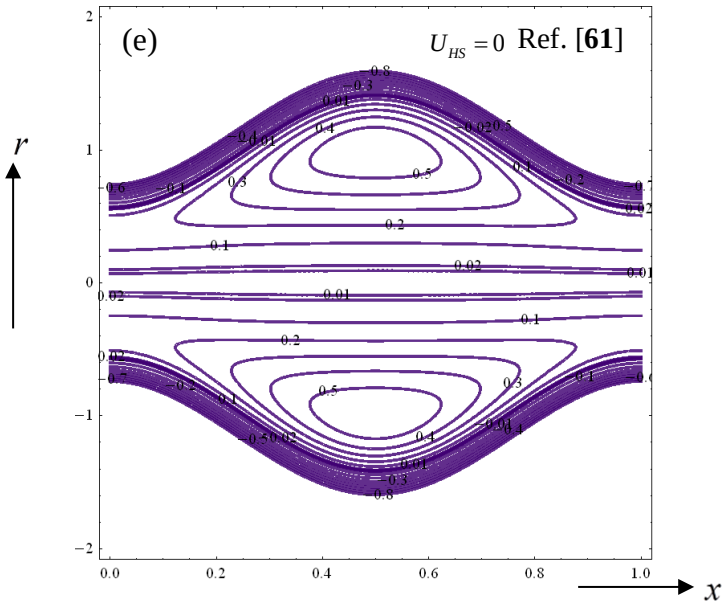

Fig.8. Stream lines in wave form at $\phi = 0.6, \bar{Q} = 0.7$ for different electroosmotic and Helmholtz-Smoluchowski velocity parameters.

The length of tube is twice of wavelength. The local wall shear stress distribution is *U*-shaped, with a maximum at the initial stage. It is reduced when the vessel walls start relaxing and constant for the relaxed phase of walls. It again increases when the walls start to contract. A similar behaviour is observed for both successive waves in the case of train wave propagation also in the single wave propagation scenario. Increasing axial electrical field i.e. greater Helmholtz-Smoluchowski velocity clearly *damps the peristaltic flow* i.e. causes a *strong deceleration*. The flow is therefore accelerated in the case of vanishing electrical field (U_{HS}=0).

Figs. 6(a-c) illustrates that effects of tube length (*axial distance*, *x*), electro-osmotic parameter (i.e. reciprocal of Debye length), and combined electro-osmotic parameter and Helmholtz-Smoluchowski velocity (external axial electric field) on the variation of volume flow rate against time for single wave propagation. Fig. 6a reveals that the variation of flow rate is oscillatory in nature and it is dependent on a set of values of time and tube length. It is also seen that the inlet flow rate is zero at initial stage (inlet flow rate) and alternates with progression in time and tube length and finally reduces again to zero (outlet flow rate). Fig.6b depicts that volume flow rate enhances with reducing the magnitude of EDL thickness (i.e. the value of electro-osmotic parameter, m from 1-50) and ascends to values very close to the flow rate for very thin EDL ($m \to \infty$). Fig. 6c shows that the effect of external electric field on volume flow rate with EDL thickness effect. It is found that flow rate diminishes with

increasing effects of external electric field (smaller Debye lengths) and furthermore for low value of Debye length, the flow rate is very close to the case of very thin EDL.

Figs. 7(a & b) are drawn to illustrate the pressure difference across the one wavelength against the time averaged flow rate under the influences of electro-osmotic parameter (thickness of EDL) and external electric field. It is observed that the relation between pressure difference and flow rate is *linear* and the pressure is maximized at zero flow rate and vice-versa. With greater flow rate the pressure decreases. Fig. 7a shows that the pressure ascends and approaches that for very thin EDL (i.e. $m \to \infty$) with increasing the magnitude of m from 0-50 that means the pressure enhances with reducing the thickness of EDL. Fig.6b shows that the pressure rises with increasing the effects of external electric field and it is minimum for without external electric field. The pressure without electric field is similar in pattern to the results of Shapiro *et al.* **[61].**

Figs.8 (a-g) present the collective effects of electro-osmotic parameter (m) i.e. thickness of EDL and Helmholtz-Smoluchowski (U_{HS}) i.e. external electric field on trapping phenomena. Furthermore we compare with the trapping phenomenon obtained in the case of *very thin* EDL i.e. with absence of electro-osmotic effect which is the case examined by Shapiro *et al.* **[56].** Trapping is special characteristic associated with peristaltic pumping and involves the localization of zones of vorticity i.e. circulation which are trapped in the flow. We have studied this phenomenon with a representative combination of the values of amplitude of peristaltic wave and time averaged flow rate. Figures are plotted for stream lines (radial coordinate vs axial coordinate) at characteristic values of amplitude and averaged flow rate i.e. $\phi = 0.6, \bar{Q} = 0.7$ encountered in real blood flows. Figs**. 8(a-d)** illustrate that the effects of external electric field on trapping for both cases with finite Debye length (i.e. $m = 10$) and very thin EDL (i.e. $m \to \infty$). It is apparent that the size of trapped bolus reduces with increasing the effects of external electric field. From **Figs. 8(a & b)** and (c & d), the stream lines are very similar for both cases $m = 10$ and $m \to \infty$ but the similarity is progressively lost when external electric field is stronger. **Figs.8 (c, e)** show the variation in Debye length at $U_{HS} = 0.1$, and it is observed that the size of trapped bolus reduces with decreasing the magnitude of Debye length (i.e. increasing value of electro-osmotic parameter, m).

4. CONCLUSIONS

A theoretical study has been conducted for the unsteady peristaltic pumping of electro-osmotic viscous blood flow in a finite length cylindrical vessel. The classical Navier-Stokes (Newtonian) fluid model has been employed. Using lubrication and Debye-Hückel linearization approximations, closed-form solutions for the normalized and linearized boundary value problem have been derived for axial velocity, pressure gradient or difference, volumetric flow rate and local wall shear stress. The influence of vessel length, time, electro-osmotic parameter (inverse Debye length) and Helmholtz-Smoluchowski velocity (proportional to axial electric field) on pumping characteristics has been evaluated. Trapping bolus dynamics has also been studied both with and without electro-kinetic effects. Also a comparative examination of train wave propagation and single wave propagation under the effects of thickness of electrical double layer (EDL) and external electric field has been included. The present computations, obtained via Mathematica software have shown that:

- **(i)** Maximum blood pressure arises for fully contracted walls whereas the minimum is associated with fully relaxed walls.
- **(ii)** It is also observed that the pressure is reduced with electro-osmotic parameter i.e. increases with increasing the thickness of Debye length in *train wave propagation* with the converse response observed for single wave propagation.
- **(iii)** Owing to contraction and relaxation of walls, a *negative pressure gradient* is generated which sustains propagation of the blood bolus (trapped vorticity zone) in the forward axial direction.
- **(iv)** Pressure is *significantly suppressed with greater* external electrical field i.e. larger values of the Helmholtz-Smoluchowski velocity, for *train wave propagation; the contrary behaviour is the case* for single wave propagation.
- **(v)** Similar patterns are computed for pressure distribution to the non-osmotic blood flow study of Li and Brasseur [**36**] i.e. without external electric field.
- **(vi)** With progression in time, there is a substantial reduction in wall shear stress which exhibits a U-shaped profile (and therefore associated axial flow retardation) with increasing electro-osmotic parameter (i.e. decreasing Debye electrical length).
- **(vii)** Periodic distributions in wall shear stress are strongly evident indicating the wavy nature of peristaltic propulsion.

(viii) Local wall shear stress distribution is maximized at the initial stage of propulsion and is depressed with wall contraction and constant for wall relaxation, for both train wave propagation also single wave propagation cases.

(ix) Larger strength of axial electrical field i.e. greater Helmholtz-Smoluchowski velocity, significantly decelerates the peristaltic blood flow.

(x) An absence of electrical field accelerates the blood flow indicating that *with electrical field* hemodynamic control is achieved.

(xi) With increasing electro-osmotic parameter (decreasing Debye length), volume flow rate is elevated, tending to the value for very thin EDL (as electro-osmotic parameter tends to infinity).

(xii) Flow rate is reduced with stronger Helmholtz-Smoluchowski velocity i.e. stronger external axial electric field.

(xiii) A linear decay relation is computed between pressure difference and flow rate.

(xiv) Pressure is boosted with stronger axial electric field and it is a minimum without external electric field. The pressure distributions in the absence of electric field resemble those computed by *et al.* [**61**].

(xv) Bolus magnitude is reduced with increasing axial external electric field and also with greater electro-osmotic parameter (smaller Debye length).

An important pathway for extending the current linearized two-dimensional simulations is to deploy computational fluid dynamics (CFD) software for *transient 3-D simulations*. An excellent suite available for modelling such flows is the **ANSYS FLUENT** code. This has been implemented by Laskowski and Bart [**62**] in conjunction with **openFOAM** algorithms to analyse electro-kinetic flow dynamics in chromatographic devices. Other softwares which have been utilized to simulate electro-kinetic dynamics include the **SIMION** code and the finite element code, **COMSOL** Multi-physics [**63**]. These simulations have explored ion motion at elevated pressure calibrated against experimentally derived ion current data. Peristaltic computational fluid dynamics studies include Tharakan *et al*. [**64**] with applications in gastric transport; however electrokinetics has not been considered. Therefore to the authors' knowledge composite electro-kinetic peristaltic hemodynamics has thusfar not been analyzed with general purpose CFD softwares. However recently El Gendy [**65**] has explored peristaltic flows in smart pumps using **ANSYS FLUENT** and also considered both Newtonian and non-Newtonian models. These studies may be further extended to consider combined models using the Navier–Stokes equations, energy equations for stationary

temperature fields and mass transfer equations for the electrokinetic flow. Another aspect of significance which has been ignored in the present simulation is heat transfer. The heat-conducting properties of blood make this an important feature to analyse in capillary electro-osmotic flows. Furthermore this provides other key aspects of interest including entropy generation minimization via second law thermodynamic simulation. Important studies in this regard have been presented by Gorla [**66**] for micro-channels and Goswami *et al.* [**67**] for conjugate electro-osmotic heat transfer. These models have however only considered Newtonian flows. Non-Newtonian characteristics may feature strongly in micro-capillary transport. Important constitutive models which could be considered therefore include power-law models [**68**], micropolar models [**69**] and couple stress models [**70**]. These would provide more comprehensive insight into non-Newtonian biological entropy simulation in electro-osmotic peristalsis and indeed both *couple stress* [**71**] and *viscoelastic* models [**72**] are currently being explored.

ACKNOWLEDGEMENTS

The authors are extremely grateful to all the reviewers for their insightful comments which have served to improve the present work and have also identified substantial pathways for future developments.

REFERENCES

[1] A.R. Minerick, A.E. Ostafin and H.C. Chang, Electrokinetic transport of red blood cells in microcapillaries. *Electrophoresis*. 14 (2002) 2165-73.

[2]M. Macka *et al.*, Poly(tetrafluoroethylene) separation capillaries for capillary electrophoresis. Properties and applications, *J. Chromatogr A.*, 1039 (2004) 193-9.

[3] D. P. Trivedi, K. J. Hallock, P. R. Bergethon, Electric fields caused by blood flow modulate vascular endothelial electrophysiology and nitric oxide production, *Bioelectromagnetics,* 34 (2013) 22–30.

[4] E.H. Serpersu, T.Y. Tsong, Activation of electrogenic Rbþ transport of (Na,K)-ATPase by an electric field, *J. Biol. Chem* 259 (1984) 7155–7162.

[5] X. Xing, M. He, H. Qiu and L. Yobas Continuous-flow electrokinetic-assisted plasmapheresis by using three-dimensional microelectrodes featuring sidewall undercuts, *Anal. Chem*., 88 (2016) 5197−5204.

[6] M. Washizu and O. Kurosawa, Electrostatic manipulation of DNA in microfabricated structures, *IEEE Trans. Ind. Appl*. 26 (1990) 1165–1172.

[7] M. Washizu, S. Suzuki, O. Kurosawa, T. Nishizaka, and T. Shinohara, Molecular dielectrophoresis of biopolymers. *IEEE Trans. Ind.Appl*., 30 (1994) 835– 843.

[8] S. Ghosal, Electrokinetic flow and dispersion in capillary electrophoresis, *Ann. Rev. Fluid Mechanics*, 38 (2006) 309-338.

[9] A. Sonnenberg et al., Rapid Electrokinetic isolation of cancer-related circulating cell-free DNA directly from blood, *Clinical Chemistry*, 60 (2014) 500-509.

[10] Sharp, K. A. and Honig, B. Electrostatic interactions in macromolecules: theory and applications. *Annual Review of Biophysics and Biophysical Chemistry*, 19 (1990) 301–332

[11] W.K. Liu *et al.*, Immersed molecular electrokinetic finite element method for nano-devices in biotechnology and gene delivery, *Meshfree Methods for Partial Differential Equations VI, Lecture Notes in Computational Science and Engineering*, 89 (2012) 67-74.

[12] D. Hlushkou, Kandhai, D., and Tallarek, U. Coupled lattice-Boltzmann and finite-difference simulation of electroosmosis in microfluidic channels, *Int. J. Numerical Methods in Fluids*, 46 (2004) 507–532.

[13]T.W.H. Sheu, Huang, V. C., and Rani, H. P. Development of an electroosmotic flow model to study the dynamic behaviour in human meridian, *Int. J. Numerical Methods in Fluids*, 56 (2008) 739–751.

[14] B. Gheshlaghi, H. Nazaripoor, A. Kumar and M. Sadrzadeh, Analytical solution for transient electroosmotic flow in a rotating microchannel, *RSC Adv.*, 6 (2016) 17632-17641.

[15] J. G. Santiago, Electro-osmotic flows in microchannels with finite inertial and pressure forces, *Anal. Chem.*, 73 (2001) 2353-2365.

[16] J. M. Alam, J. M. Penney, A Lagrangian approach for modelling electro-kinetic mass transfer in microchannels, *Int. J. Heat and Mass Transfer*, 55 (2012) 7847–7857.

[17] X. Luo, A. Beskok, G.E. Karniadakis, Modeling electrokinetic flows by the smoothed profile method, *J. Comp. Physics*, 229 (2010) 3828-3847.

[18] O. Anwar Bég, M. Hameed and T.A. Bég, Chebyschev spectral collocation simulation of nonlinear boundary value problems in electrohydrodynamics, *Int. J. Computational Methods in Engineering Science and Mechanics*, 14 (2013) 104-115.

[19] V. C. Huang, T. W.H. Sheu, Tissue fluids in microchannel subjected to an externally applied electric potential, *Int. J. Numerical Methods for Heat & Fluid Flow*, 19 (2009) 64 – 77.

[20] E. Karatay, C. L. Druzgalski, A. Mani, Simulation of chaotic electrokinetic transport: Performance of commercial software versus custom-built direct numerical simulation codes, *J. Colloid and Interface Science*, 446 (2015) 67–76.

[21]M. M**o**ndal, R.P. Misra and S. De, Combined electroosmotic and pressure driven flow in a microchannel at high zeta potential and overlapping electrical double layer**,** Int**.** J**.** Thermal Sciences**,** 86 (2014) 48-59.

[22] C. de Loubens, Albert Magnin, Eric Verin, Marion Doyennette, Ioan Cristian Tréléa, Isabelle Souchon, A lubrication analysis of pharyngeal peristalsis: Application to flavour release, *J. Theoretical Biology*, 267 (2010) 300-311.

[23] A. Farina, L. Fusi, A. Fasano, A. Ceretani, F. Rosso, Modeling peristaltic flow in vessels equipped with valves: Implications for vasomotion in bat wing venules, *Int. J. Engineering Science*, 107 (2016) 1-12.

[24] K. K. Bokka, Edwin C. Jesudason, David Warburton, Sharon R. Lubkin, Morphogenetic implications of peristaltic fluid–tissue dynamics in the embryonic lung, *J. Theoretical Biology*, 382 (2015) 378-385.

[25] S. Maiti, J.C. Misra, Peristaltic flow of a fluid in a porous channel: A study having relevance to flow of bile within ducts in a pathological state, *Int. J. Engineering Science*, 49 (2011) 950-966.

[26] D. Tripathi and O. Anwar Bég, Mathematical modelling of peristaltic pumping of nano-fluids, *Modelling and Simulation of Diffusive Processes, Simulation Foundations, Methods and Applications*, Springer, Germany, 69-95 (2014).

[27] M. Costa and Furness, J. B., The peristaltic reflex: an analysis of the nerve pathways and their pharmacology. *Naunyn Schmiedebergs Arch. Pharmacol*., 294 (1976) 47-60.

[28] I. Rönnestad, Rojas-Garcia, C. R. and Skadal, J., Retrograde peristalsis; a possible mechanism for filling the pyloric caeca*? J. Fish Biol*., 56 (2000) 216-218.

[29] K. A Daltorio, Alexander S Boxerbaum, Andrew D Horchler, Kendrick M Shaw, Hillel J Chiel and Roger D Quinn, Efficient worm-like locomotion: slip and control of soft-bodied peristaltic robots, *Bioinspir. Biomim.,* 8 (2013) 035003.

[30] R J Lock, S C Burgess and R Vaidyanathan, Multi-modal locomotion: from animal to application, *Bioinspir. Biomim.,* 9 (2014) 011001.

[31] F. Yin and Y.C. Fung, Peristaltic waves in a circular cylindrical tube, *ASME J. Applied Mech.,* 36 (1969) 93-112.

[32] S.L. Weinberg, Eckistein EC, Shapiro AH. An experimental study of peristaltic pumping, *J. Fluid Mech*., 49 (1971) 461-497.

[33] D. Tang and S. Rankin, Numerical and asymptotic solutions for peristaltic motion of nonlinear viscous flows with elastic free boundaries, *SIAM J. Sci. Comput*., 14 (1993) 1300-1319.

[34] E.O. Carew and T.J. Pedley, An active membrane model for peristaltic pumping: part 1 - periodic activation waves in an infinite tube, *ASME J. Biomech. Engng.,* 119 (1997) 66-76.

[35] D. Tang, M.C. Shen, Peristaltic transport of a heat-conducting fluid subject to Newton's Cooling law at the boundary, *Int. J. Engineering Science*, 27 (1989) 809-825.

[36] M. Li and J. G. Brasseur, Non-steady peristaltic transport in finite-length tubes, *J. Fluid Mechanics*, 248, 129-151 (1993).

[37] Y. V. K. Ravi Kumar, S. V. H. N. Krishna Kumari, P. M. V. Ramana Murthy and S. Sreenadh, Unsteady peristaltic pumping in a finite length tube with permeable wall, *ASME J. Fluids Eng.,* 132 (2010) 101201.

[38] D. Tripathi and O. Anwar Bég, A study of unsteady physiological magneto-fluid flow and heat transfer through a finite length channel by peristaltic pumping, *Proc. Inst. Mech. Eng H.- J. Engineering in Medicine*, 226 (2012) 631-44.

[39] E. Toklu, A new mathematical model of peristaltic flow on esophageal bolus transport, *Scientific Research and Essays,* 6 (2015), 6606-6614.

[40] J. C. K. Tong, Ephraim M. Sparrow and John P. Abraham, Numerical simulation of the urine flow in a stented ureter, *ASME J Biomech. Eng* 129 (2006) 187-192.

[41] A. Pal and J. G. Brasseur, The mechanical advantage of local longitudinal shortening on peristaltic transport, *ASME J. Biomech. Eng* 124 (2001) 94-100.

[42] C. Jaggy *et al*., Affinity pump system: a new peristaltic blood pump for cardiopulmonary bypass, *Perfusion*, 15 (2000) 77-83.

[43] D. Tripathi, and O.A. Bég, Transient magneto-peristaltic flow of couple stress biofluids: a magneto-hydro-dynamical study on digestive transport phenomena, *Mathematical Biosciences*, 246 (2013) 72-83.

[44] A. Bandopadhyay, D. Tripathi and S. Chakraborthy, Electro-osmosis-modulated peristaltic transport in microfluidic channels, *Physics of Fluids*, 28 (2016) 052002.

[45] Misra, J.C., Chandra, S., *Appl. Math. Mech.-Engl. Ed*. 35 (2014) 749766.

[46] D. Tripathi, S. Bhushan and O. Anwar Bég, Transverse magnetic field driven modification in unsteady peristaltic transport with electrical double layer effects, *Colloids and Surfaces A: Physicochemical and Engineering Aspects*, 506 (2016) 32–39.

[47] P. Goswami *et al*, Electrokinetically modulated peristaltic transport of power-law fluids, *Microvascular Research*, 103 (2016) 41–54.

[48] D.G. Johnson, Integration technologies for implantable microsystems, *PhD Thesis, Microsystems Engineering, Department of Electrical Engineering, Rochester Institute of Technology Rochester, New York, USA* (2013).

[49] T.E. McKnight, C.T. Culbertson, S.C. Jacobson, J.M. Ramsey, Electro-osmotically induced hydraulic pumping with integrated electrodes on microfluidic devices, *Anal. Chem.*, 73 (2001) 4045-4049.

[50] Czosnyka M, Piechnik S, Richards HK, Kirkpatrick P, Smielewski P, Pickard JD. Contribution of mathematical modelling to the bedside tests of cerebrovascular autoregulation, *J. Neurology, Neurosurgery, and Psychiatry,* 63 (1997) 721-731.

[51] D.S. Reichmuth, Chirica GS, Kirby B.J., Increasing the performance of high-pressure, high-efficiency electrokinetic micropumps using zwitterionic solute additives, *Sensors and Actuators B-Chemical*, 92 (2003) 37-43.

[52]B.G. Hawkins, Gleghorn JP, Kirby B.J., Dielectrophoresis for cell and particle manipulations, *Methods in Bioengineering: Biomicrofabrication and Biomicrofluidics*, Ed. J.D. Zahn, Artech Press, USA (2009).

[53]H. Ginsburg, Analysis of plant root electro-potentials, *J. Theoretical Biology*, 37 (1972) 389-412.

[54] Quincke G, On the continuation of material particles by the flow of electricity, *Ann. Phys*., 189:513–598 (1861).

[55] Serpersu EH, Tsong TY. Activation of electrogenic Rb^+ transport of (Na,K)-ATPase by an electric field. *J Biol. Chem*. 259:7155–7162 (1984).

[56] Astumian RD, Robertson B. Nonlinear effect of an oscillating electric field on membrane proteins. *J Chem Phys*.91:4891–4901 (1989).

[57] Gardner SE, Frantz RA, Schmidt FL, Effect of electrical stimulation on chronic wound healing: a meta-analysis, *Wound Repair Regen*. **7** (6): 495–503 (1999).

[58] Kochetkov AV, Gorbunov FE, The hemodynamic effects of transcerebral electro- and electromagnetotherapy in stroke patients, *Vopr Kurortol Fizioter Lech Fiz Kult*. 1999 Jul-Aug;(4):17-21.

[59] D.A. Saville, Electrokinetic effects with small particles, *Ann. Rev. Fluid Mechanics*, 9 (1977) 321-337.

[60] E. Kreyzig, *Advanced Engineering Mathematics*, Wiley, New York (1980).

[61] A. H. Shapiro, M. Y. Jaffrin And S. L. Weinberg, Peristaltic pumping with long wavelengths at low Reynolds number, *J. Fluid Mech*., 37 (1969) 799-825.

[62] R. Laskowski, Hans-Jörg Bart, Electroosmotic flow and Joule heating in preparative continuous annular electrochromatography, *Electrophoresis*, 36, 2128–2137 (2015)

[63] W. Wissdorf, Larissa Pohler, Sonja Klee and Thorsten Benter, Simulation of ion motion at atmospheric pressure: particle tracing versus electrokinetic flow, *J. American Society Mass Spectrometry*, 23(2):397-406 (2011).

[64] A. Tharakan, I.T. Norton, P.J. Fryer, S. Bakalis, Mass transfer and nutrient absorption in a simulated model of small intestine. *J. Food Science*, 75 (6), E339-E346 (2010).

[65] M. El Gendy, ANSYS Fluent CFD simulation of peristaltic smart pumps, *MSc Thesis Aerospace Engineering, Salford University, Manchester, UK, August* (2016).

[66] R.S.R Gorla, Entropy generation in electro-osmotic flow in microchannels, *Int. J. Micro-Nano Scale Transport*, 4, (1), 1-10 (2014).

[67] Prakash Goswami, Pranab Kumar Mondal, Anubhab Datta and Suman Chakraborty, Entropy generation minimization in an electroosmotic flow of non-newtonian fluid: effect of conjugate heat transfer, *ASME J. Heat Transfer* 138(5), 051704 (Feb 03, 2016) (9 pages).

[68] C-H. Chen, Electro-osmotic heat transfer of non-Newtonian fluid flow in microchannels, *ASME J. Heat Transfer* 133(7), 071705 (2011).

[69] J.V. Ramana Murthy and S. Jangili, Second law analysis for Poiseuille flow of immiscible micropolar fluids in a channel, *Int. J. Heat Mass Transfer* 65, 254-264 (2013).

[70] S Jangili, JV Ramana Murthy, KS Sai, Entropy generation analysis of the flow of two immiscible couple stress fluids between two porous beds, *Comp. Thermal Sciences:* 7 (2), 123-137 (2015).

[71] D. Tripathi, A. Yadav and O. Anwar Bég, Electro-osmotic flow of couple stress fluids in a micro-channel propagated by peristalsis, *Applied Mathematical Modelling* (2016). **communicated.**

[72] D. Tripathi, A. Yadav and O. Anwar Bég, Electro-kinetically driven peristaltic transport of viscoelastic biofluids through a capillary: mathematical modelling, *Mathematical Biosciences* (2016). **communicated.**